Received June 14, 2020, accepted July 14, 2020, date of publication July 23, 2020, date of current version August 13, 2020.

Digital Object Identifier 10.1109/ACCESS.2020.3011569

Analysis of Transport and Mixing Phenomenon to Invariant Manifolds Using LCS and KAM Theory Approach in Unsteady Dynamical Systems

RIAZ AHMAD[1], ASMA FAROOQI[1], JIAZHONG ZHANG[1], ILYAS KHAN[2], AND EL-SAYED M. SHERIF[3,4]

[1]School of Energy and Power Engineering, Xi'an Jiaotong University, Xi'an 710049, China
[2]Faculty of Mathematics and Statistics, Ton Duc Thang University, Ho Chi Minh 72915, Vietnam
[3]Mechanical Engineering Department, College of Engineering, King Saud University, Riyadh 11421, Saudi Arabia
[4]Electrochemistry and Corrosion Laboratory, Department of Physical Chemistry, National Research Centre, Cairo 12622, Egypt

Corresponding author: Ilyas Khan (ilyaskhan@tdtu.edu.vn)

This work was supported by Researchers Supporting Project Number (RSP-2020/33), King Saud University, Riyadh, Saudi Arabia.

ABSTRACT The Lagrangian approach for the two-dimensional incompressible fluid flows has been studied with the help of dynamical systems techniques: Kolmogorov-Arnold-Moser (KAM) theory, stable, unstable manifold structures, and Lagrangian coherent structures (LCSs). For the time-dependent perturbation problems, we analyze in detail the development of transport barriers that play an important role in the transport process. Firstly, the analytical study of KAM theory is adopted to explain the transport and mixing phenomenon in measured and simulated airfoil flow. Then, the flow topology of unsteady flow behind an airfoil is investigated for the low Reynolds number problem. Simulations are carried out based on a particular Finite-Time Lyapunov Exponent (FTLE) technique for the detection of invariant manifolds of the hyperbolic trajectories. Besides, the Characteristic Base Split (CBS) scheme combined with a dual time stepping technique is utilized to simulate such transient flow problems. Thus, in the course of the current research, the role of the velocity phase plot during vortex formation is explored that is highly periodic and resulted in the formation of a stable pattern of manifolds and invariant tori. Hence, the proposed study encouraged the new picture of the vortex shedding and flow separation process. As a conclusion, our results give a better understanding of invariant tori control transport phenomena that will lead to a new heuristic for unsteady flows.

INDEX TERMS CBS method, Hamiltonian dynamics, KAM theory, Lagrangian coherent structures, nonlinear dynamics, transport phenomena.

I. INTRODUCTION

Understanding the dynamics of transport and mixing phenomenon is an immediate imposing challenge in the multidisciplinary areas of science and engineering [1]–[4]. Dynamical systems tools, such as KAM theory and LCS, revealed the evolvement of fluid parcels in the flow of interest. The significance of these structures near the neighborhood flow is their transport barrier behavior. The Lagrangian approach of hyperbolic trajectories has been examined in many fluid problems in the last few decades [5], [6].

For the dynamical system theory, invariant manifolds of hyperbolic trajectories have become more informative for well-defined structures in the flow field. So, a Poincare map for time-periodic flows is constructed to reveal such KAM tori. The study of these structures attains much importance in fluid dynamics because they serve as transport barriers particularly in regular regions of the flow. In KAM tori, mixing is restrained and the coherent regions are formed [7]–[9]. While, in the case of LCS, mixing is enhanced because of the stretching and folding nature of neighboring elements [10], [11].

Much of the work on dynamical system tools have explained some kind of structures, called LCS's [12]. These structures influenced the geometry of the mixing of fluids. In 2000 Haller [13] presented a concept of a Lagrangian analysis which revealed the finite time material lines by computing the FTLE in the velocity field. The expanding divergence

The associate editor coordinating the review of this manuscript and approving it for publication was Ming Xu.

of nearby trajectories in the flow can be determined by FTLE. As the particle arrangement is linear in kinematic fluid, the FTLE is determined in backward/forward time. FTLE measures the stretching and contraction of the fluid for forward and backward time respectively. It is considered that attracting and repelling barriers formed by the backward and forward time of FTLE contours respectively. Mixing of these barriers revealed the true picture of LCSs. Combination of a repelling and attracting transport barrier encompassing a circulating fluid present a good identifier of a vortex [14]. The deformity of FTLE confinement over time is involved in determining coherent structures and the mechanism of fluid entrainment for time-dependent flow [15], [16].

Many techniques have been developed and applied to identify LCS in the various oceanic and atmospheric flows [17]–[19]. Two of these techniques are very important. The first one is stable and unstable manifolds of hyperbolic trajectories that define chaotic transport in time-dependent flows [20]–[23]. The second one is known as invariant KAM tori, which has been associated with regular regions of constrained transport [18]. Rypina *et al.* [24] have used the true approach of dynamical systems like KAM theory, stable/unstable manifolds, lobe dynamics, and its transformation. An analytical approach has been studied to express the much attention of KAM invariant tori, stable/unstable manifolds, and the behavior by which these structures restraint transport. These tools and concepts of dynamical systems are helpful and insightful in studies of fluid transport [25]. Present literature has attained much attention to the Lagrangian description of the transport and mixing of fluids about coherent structures. Researchers preferred to use the Lagrangian approach of the fluid and illustrate the non-linear dynamics behavior of the flow. Van Dommelen *et al.* [26] have worked on unsteady boundary layer equation and they studied the flow separation criteria through the Lagrangian way. Wiggins *et al.* [27] have explained the mass transport and vortex formation adjacent to the wake of a circular cylinder by using manifolds theorem and lobe structure. However, a non-linear dynamics approach can be applied for infinite time flow by using a traditional manifold. Haller [13] has analyzed the approach of LCSs and finite time manifolds and discuss the boundaries of the vortex in finite time flow. Researchers are convenient to apply the Lagrangian method to investigate fluid transport and unsteady separation. A wide range of flow phenomena, such as biological phenomena [28], turbulent flows [29], vortex shedding [30], geophysical flows [31], etc, have been studied by LCS.

The paper objectives are summarized with the following: (i) to review KAM theory for better understanding the behavior of nearly integrable Hamiltonian systems, (ii) the Lagrangian Coherent Structure is introduced to understand the Lagrangian dynamics of the flow process, such as vortex shedding and the separation bubble, (iii) a numerical method is introduced to simulate the flow around the airfoil. Finally, we present the summary of the results and conclusions.

II. KAM THEORY FORMULATION

Last few decades, the importance of KAM theory has been increased, especially for the cognizance of the behavior of non-integrable Hamiltonian systems. Nonlinear Hamiltonian systems having complex motion can be analyzed extensively by KAM theory. The dynamics of the perturbed Hamiltonian systems is not performed well for the separable dynamical systems that lead to the KAM theory formulation. For non-integrable systems, fluid trajectories presents complicated behavior until it becomes integrable.

In this work, we consider the equations of motion in the velocity field as

$$\dot{\mathbf{P}} = \mathbf{v}(\mathbf{P}, t), \tag{1}$$

where $\mathbf{P} = (x, y, z)$ and $\mathbf{v} = (u, v, w)$ are the position and velocity at (x, y, z).

For incompressible flow, the components of velocity can be defined in the form of a stream function. Hamiltonian form of the equation of motion (2) can be given as

$$\dot{x} = -\frac{\partial \psi}{\partial y}(x, y, t), \qquad \dot{y} = \frac{\partial \psi}{\partial x}(x, y, t), \tag{2}$$

where $\psi(x, y, t)$ considers as the Hamiltonian equation and (x, y) are the phase space coordinates in fluid flow.

Now we consider the stream function as

$$\psi(x, y, t) = h(x, y) + r(x, y, \Omega_1 t, \ldots, \Omega_N t). \tag{3}$$

where r is a multi-periodic function having periods $\frac{2\pi}{\sigma_i}$, $i = 1, 2, \ldots, N$.

The perturbation stream function in bounded domain is expressed as

$$\psi(x, y, t) = A_o(y) + \sum_{1}^{(N+1)} A_n(y) cos\big[k_n(x - c_n t) + \phi_n\big]. \tag{4}$$

In a reference frame, time dependence is eliminated from the flow. So the stream function at speed $C_{(N+1)}$ is written as

$$\Psi(\hat{x}, y, t) = H(\hat{x}, y) + R(\hat{x}, y, \Omega_1 t, \ldots, \Omega_N t), \tag{5}$$

where $\hat{x} = x - C_{(N+1)} t \; mod 2\pi \, acos\theta_o$ is the wave co-moving zonal coordinates. And

$$H = C_{(N+1)} y + A_o(y) + A_{(N+1)}(y) cos(k_{N+1}\hat{x} + \phi_{(N+1)}), \tag{6}$$

$$R = \sum_{1}^{N} A_n(y) cos\big[k_n \hat{x} - \Omega_n t + \phi_n\big], \tag{7}$$

where $\Omega_n = k_n(c_n - c_{(N+1)})$

Hence, fluid-particle motion complying Eq. (2) reduce to the integrable system, using the stream function of type (5-7) and KAM theory can handle such systems.

Further, action-angle (I, θ) variables are introduced in a piecewise way. These variables exist when the energy level set is compact and flows are complete. They give the most concise explanation and easily applied to the KAM theory results.

The canonical remodeling $(y, x) \mapsto (I, \theta))$ is expressed as

$$I = \frac{1}{2\pi} \oint \hat{X}(y; H)dy, \tag{8}$$

$$\theta = \partial_1 G, \tag{9}$$

$$G(y, I) = \int_0^y \hat{X}(\xi; H)d\xi. \tag{10}$$

Hence, the back ground and perturbed Hamiltonian, respectively, defined as

$$H(\hat{x}, y) = \mathcal{H}(I),$$
$$R(\hat{x}, y, \Omega_1 t, \ldots, \Omega_N t) = \mathcal{R}(I, \theta, \Omega_1 t, \ldots, \Omega_N t). \tag{11}$$

The action-angle variables (I, θ) expansion as

$$\dot{I} = -\partial_\theta \mathcal{R}, \quad \dot{\theta} = \omega(I) + \partial_1 \mathcal{R}, \tag{12}$$

where

$$\omega(I) = \acute{\mathcal{H}}. \tag{13}$$

The Hamiltonian $\mathcal{H}$ is the first integral, when $\mathcal{R} = 0$, and the motion defined by Eqs. (11-13) is completely integrable. Trajectories are then shown on one dimensional tori $I = constant$.

Under perturbation, it is studied the special form of unperturbed tori $(\omega'(I) = 0)$ which are resistant to break [3]. This form of stability is recognized as strong KAM stability.

Consider a Hamiltonian system

$$\dot{I} = -\frac{\partial H}{\partial \theta}, \quad \dot{\theta} = \frac{\partial H}{\partial I}. \tag{14}$$

And the Hamiltonian

$$H(I, \theta, t) = H_o(I) + \epsilon H_1(I, \theta, \Omega_1 t, \ldots, \Omega_N t). \tag{15}$$

The perturbation $H(I, \theta, t)$ in Eq. (15) is multi-periodic and its Fourier series is written as

$$H_1(I, \theta, t) = \sum_{m,n=-\infty}^{\infty} K_{nm}(I) cos(n\theta - m\Omega t + \phi_{nm}), \tag{16}$$

where the $\phi_{nm}s$ are the phases. The equations of motion is defined as

$$\dot{I} = \epsilon \sum_{m,n=-\infty}^{\infty} nK_{nm}(I) sin(n\theta - m\Omega t + \phi_{nm}) \tag{17}$$

and

$$\dot{\theta} = \omega(I) + \epsilon \sum_{m,n=-\infty}^{\infty} nK'_{nm}(I) cos(n\theta - m\Omega t + \phi_{nm}). \tag{18}$$

For small ϵ, $\omega(I)$ satisfies $\omega^{(j-1)}(I_o) = 0$, $\omega^j(I_o) \neq 0$ for any integer $j \geq 2$ and $I_o \in I$.

Let $\psi = n\theta - m\Omega t + \phi_{nm}$ be the term akin to the resonant (n, m). By noting that $\dot{\psi} = n\dot{\theta} - m\Omega$ and all the oscillating values in Eqs. (17) and (18) are eliminated.

$K_{nm}(I)$ is replaced with the resonant value $K_{nm}(I_o)$ and $\omega(I)$ is to be expanded in a Taylor series around I_o with $\delta I = (I - I_o)$ and introduce the notation $\Omega_i = \frac{\omega^{(i)}(I_o)}{i!}$, $i = 0, 1, \ldots, (j-2)$.

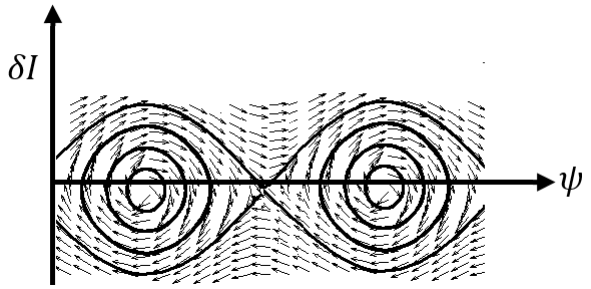

FIGURE 1. Level surfaces $(\hat{H}(\delta I, \psi))$ in the phase plane $(\psi, \delta I)$ for order of degeneracy $(j = 3)$.

The following approximate autonomous system results from Eqs. (17) and (18) in the vicinity of the resonant level:

$$\delta\dot{I} = \epsilon n K_{nm}(I_o) sin\psi, \tag{19}$$

$$\dot{\psi} = n\Big(\sigma_0 + \sigma_1 \delta I + \ldots + \sigma_{(j-2)}(\delta I)^{j-2} + \omega^j(I_0)\frac{(\delta I)^j}{j!}\Big) - m\Omega. \tag{20}$$

Higher terms in above equations has been omitted. Finally, Eqs. (19) and (20) define a Hamiltonian system

$$\delta\dot{I} = -\frac{\partial \hat{H}}{\partial \psi}, \quad \dot{\psi} = \frac{\partial \hat{H}}{\partial \delta I}. \tag{21}$$

With Hamiltonian

$$\hat{H}(\delta I, \psi) = n\left[\sigma_0 \delta I + \sigma_1 \frac{(\delta I)^2}{2} + \ldots + \omega^j(I_0)\frac{(\delta I)^{(j+1)}}{(j+1)!}\right] - m\Omega\delta I + \epsilon n K_{nm}(I_0) cos\psi \tag{22}$$

and

$$\omega(\delta I; \Omega) = \sigma_0 + \sigma_1 \delta I + \ldots + \sigma_{(j-2)}(\delta I)^{(j-2)} + \omega^j(I_0)\frac{(\delta I)^j}{(j)!}. \tag{23}$$

By defining $\Omega = \Omega_0$ with $m\Omega_0 = n\sigma_0$ and $\sigma_0 = \sigma_1 = \ldots = \sigma_{(j-2)} = 0$.

Eq. (22) reduces to

$$\hat{H}(\delta I, \psi) = n\omega^j(I_0)\frac{(\delta I)^{(j+1)}}{(j+1)!} + \epsilon n K_{nm}(I_0) cos\psi. \tag{24}$$

In Fig. 1, trajectories are trapped in the resonance region for odd values of j. Here, we define the width of resonance on a trapped region with maximum δI excursion of the separatrix

$$\Delta I = \Big(\frac{2\epsilon |K_{nm} I_0 (j+1)|}{|\omega^{(j)}(I_0)|}\Big)^{\frac{1}{(j+1)}}. \tag{25}$$

The corresponding frequency width is

$$\Delta\omega = |\omega^j(I_0)|\frac{(\Delta I)^j}{j!} = |\omega^j(I_0)|^{\left(\frac{1}{(j+1)}\right)}\left(\frac{2\epsilon |K_{nm} I_0 (j+1)|}{|\omega^{(j)}(I_0)|}\right)^{\frac{1}{(j+1)}}. \tag{26}$$

As resonances are stimulated at discrete values of ω, overlapping of resonances is only computed by the width $\Delta\omega$ rather ΔI.

From Eq. (26) it follows that degenerate resonances are generally correlated with smaller resonance widths then non-degenerate resonances. Hence, resonances around degenerate tori are expected to interwine and these regions are generally associated with enhanced stability. This phenomenon is important for the presence of robust transport barriers near non-twist trajectories in atmospheric and oceanic flows [18]. Poincaré section for a Hamiltonian system has been drawn in Fig. 2 and Fig. 3. The strength and structure of the perturbation term $\epsilon H_1(I, \theta, \Omega(t))$ in both cases are alike, but in $H_0(I)$ is different. Firstly, frequency $\omega(I)$ is cubic with two isolated ($j = 2$) degeneracies. In the other case, the frequency structure is linear. The $\omega(I)$ domain of the system is the same for both cases so excited resonances are also similar. As the resonance widths are distinct and this supports the strong stability phenomena in the locality of degenerate tori in the system having cubic frequency $\omega(I)$.

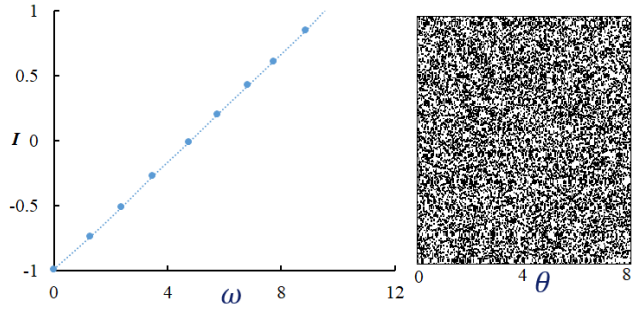

FIGURE 2. Poincaré section of Hamiltonian system for linear frequency $\omega(I)$ ($j = 2$, $\epsilon = 0.028$).

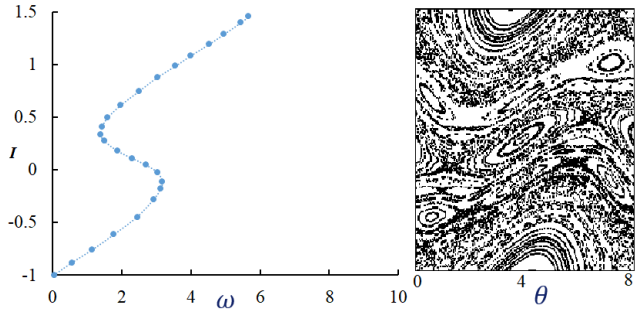

FIGURE 3. Poincaré section for Hamiltonian system for cubic frequency $\omega(I)$ ($j = 2$, $\epsilon = 0.028$).

Detection of invariant tori is complex due to the existence of the multi-periodic time dependence in the stream function. Some particular cases like simple periodic perturbation, a surface of Poincaré section could be developed to identify the presence of such structures. However, many frequencies in the perturbed stream function are large, so the FTLE technique is used for computation.

III. LAGRANGIAN COHERENT STRUCTURES

Lagrangian Coherent Structures analysis was initiated to the fluid mechanics research by Haller [1]. Attracting, repelling and shearing nature of these material surfaces would lead to the skeletons of Lagrangian particle dynamics. LCS's are considered as ridges of the FTLE field in many engineering applications [32]. Manifolds or material lines are produced by these ridges. FTLEs and LCSs can help scientists understand flow transport behaviors. The uniqueness and time dependence of these manifolds are generated by their invariance and its interaction with each other is mainly effective for fluid mixing. A flow map is to be defined for fluid particles from a position at time t_0 to the region after a finite time interval T at $(t_0 + T)$. The initial point of an individual particle at t_0 is $x(t_0) = x_0$, the particle after a time T is expressed by the flow map

$$\phi_{t_0}^{t_0+T}(x) : x(t_0) \mapsto x(t_0 + T). \tag{27}$$

FTLE can be defined as given

$$\sigma_{t_0}^{t}(x_0) = \frac{1}{2(t - t_0)} ln\lambda_{max}(t, t_0, x_0), \tag{28}$$

where $\lambda_{max}(t, t_0, x_0)$ is the eigenvalue of the deformation-gradient tensor field(also known as a Cauchy-Green strain tensor) $\sum_t(x_0, t_0)$ which is described by the following expression

$$\sum_t(x_0, t_0) = \left[\frac{\partial x(x_0, t)}{\partial x_0}\right]^T \left[\frac{\partial x(x_0, t)}{\partial x_0}\right]. \tag{29}$$

By defining the FTLE, it is revealed that repelling(attracting) LCS corresponds to maximizing curves and ridges of the FTLE field computed in forward(backward) time. The distribution of FTLE in the flow field is obtained and the contours that will visualize LCS's in the flow field are plotted. The FTLE based detection scheme is also capable of detecting barriers which are linked to surviving KAM invariant tori. Barriers of this type are associated with regular motion and thus are characterized by a generally narrow band of anomalously small values of FTLE.

IV. NUMERICAL METHOD FOR FLOW AROUND AN AIRFOIL AND DISCUSSION

Flow is incompressible and the governing Navier-Stokes equations can be expressed as

$$\frac{\partial u_i}{\partial x_i} = 0, \tag{30}$$

$$\frac{\partial u_i}{\partial t} + u_j\frac{\partial u_i}{\partial x_j} = -\frac{1}{\rho}\frac{\partial p}{\partial x_i} + \upsilon\frac{\partial^2 u_i}{\partial x_j \partial x_j} = 0, \tag{31}$$

where u_i, ρ, p and υ are the velocity components, density, pressure and kinematics viscosity respectively.

Dimensionless parameters of these quantities can be written as

$$\tilde{u_i} = \frac{u_i}{U}, \quad \tilde{x_i} = \frac{x_i}{c},$$
$$\tilde{t} = \frac{Ut}{c}, \quad \tilde{p} = \frac{p}{\rho U^2},$$

where $\rho = 1$ for incompressible flow. The non-dimensional form of the governing equations is defined as

$$\frac{\partial \tilde{u}_i}{\partial \tilde{x}_i} = 0,$$
$$\frac{\partial \tilde{u}_i}{\partial \tilde{t}} + \tilde{u}_j \frac{\partial \tilde{u}_i}{\partial x_j} = -\frac{\partial \tilde{p}}{\partial \tilde{x}_i} + \frac{1}{R_e} \frac{\partial^2 \tilde{u}_i}{\partial \tilde{x}_j \partial \tilde{x}_j},$$

where $R = \frac{Uc}{\nu}$, c is the characteristics length of airfoil, U the velocity of free stream. The non-dimensional symbol "$\sim$" of the variables in the above equation is dropped for convenience.

The dual time-stepping technique of recovering numerical solutions to transient flow around an airfoil is standard and explained by P. Nithiarasu [33]. The pseudo time is introduced that can iterate the solution in each real-time step.

The momentum equation can be defined as

$$\frac{\partial u_i}{\partial t} + \frac{\partial u_i}{\partial \tau} + u_j \frac{\partial u_i}{\partial x_j} = -\frac{\partial p}{\partial x_i} + \frac{1}{R_e} \frac{\partial^2 u_i}{\partial x_j \partial x_j} = 0, \quad (32)$$

where t is the real-time and τ is the pseudo time. The pseudo time step is used to accelerate the solution to a steady-state quickly. It addresses the addition of real-time term to the correction stage to progress in real-time.

The Navier-Stokes equations have non-linear convective terms which can leads to numerical oscillations by introducing the Galerkin finite element method. By eliminating the convection term, the numerical oscillation can be avoided. This problem can be tackled by introducing the CBS method. Further, discretization is applied along the characteristic line of the equation. The CBS algorithm can be derived in the following three steps.

Step I:

$$u_i^* = u_i^n + \Delta\tau \Big[-u_j \frac{\partial u_i}{\partial x_j} + \frac{1}{R_e} \frac{\partial^2 u_i}{\partial x_j \partial x_j} \Big]^n + \frac{\Delta\tau^2}{2} u_k^n \frac{\partial}{\partial x_k} \Big(\frac{\partial (u_j u_i)}{\partial x_j} + \frac{1}{R_e} \frac{\partial^2 u_i}{\partial x_j \partial x_j} \Big)^n. \quad (33)$$

Step II:

$$\theta \frac{\partial}{\partial x_i} \Big(\frac{\partial p^{(n+1)}}{\partial x_i} \Big) = \frac{1}{\Delta\tau} \frac{\partial}{\partial x_i} \Big(u_i^* - (1-\theta) \frac{\partial p^n}{\partial x_i} \Big). \quad (34)$$

Step III:

$$u_i^{(n+1)} - u_i^* = -\Delta\tau \frac{\partial p^{(n+\theta)}}{\partial x_i} - \Delta\tau \frac{3u_i^n - 4u_i^N + u_i^{(N-1)}}{2\Delta t}, \quad (35)$$

where $\Delta\tau$ and Δt are the pseudo and real-time, respectively. $\theta \in [0, 1]$ is the control parameter. And N and n are the pseudo and real-time steps, respectively.

Finally, the standard finite element method can be easily applied to the Eqs. [32]–[34].

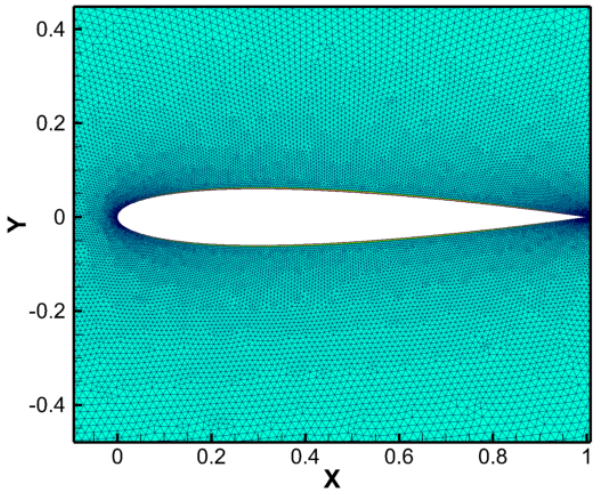

FIGURE 4. Computational mesh local view.

V. NUMERICAL RESULTS AND DISCUSSIONS

Consider a two-dimensional airfoil, NACA0012, flow is simulated numerically, and the Reynolds number is taken as 5000 which is based on the chord of the airfoil. No-slip boundary condition is taken on the airfoil surface, and the boundary condition on the boundary of the flow field is a velocity boundary condition that is set to U. The local view of fine mesh NACA0012 airfoil is shown in Fig. 4.

In order to ensure the high requirements in mesh quality, three types of meshes, which are obtained by the Easymesh program, are used at angle of attack 6°. As expected, the separated region begins farther upstream as angle of attack is increased. A closer inspection of such manifolds will show another trend. For our purpose it has been determined that the 0-9 angle of attack presents the most illustrative cases for vortex formation. As shown in Table 1, it can be seen that all of the mean lift coefficients obtained from three types of meshes are close to each other. Mesh 2 is chosen as the computational mesh in following studies.

TABLE 1. Lift coefficient at $\alpha = 6°$ and $Re = 5000$.

Mesh	nodes	elements	lift coefficient
Mesh 1	21630	42685	0.6421
Mesh 2	32108	63606	0.6397
Mesh 3	36255	71750	0.6388

A. VERIFICATION OF NUMERICAL METHOD

In Fig. 5, lift coefficient (C_l) is shown for the various angle of attack and good alignment with the experimental data [34]. It is observed that values of C_l are uniformed with the experimental value within the range of angle of attack (AOA) between $0° - 9°$. Our results simulation complies well with

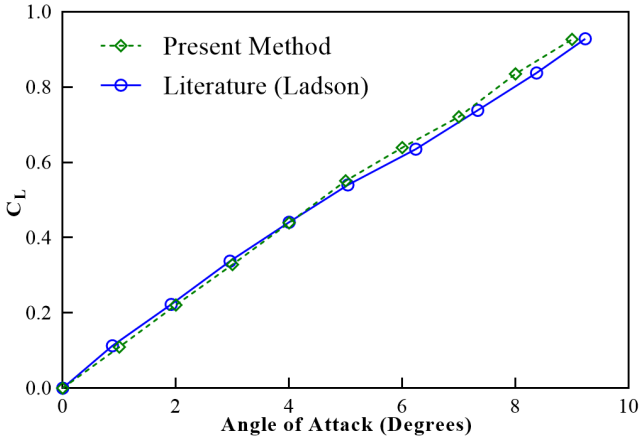

FIGURE 5. Variation of lift coefficient (C_l) for various angle of attack.

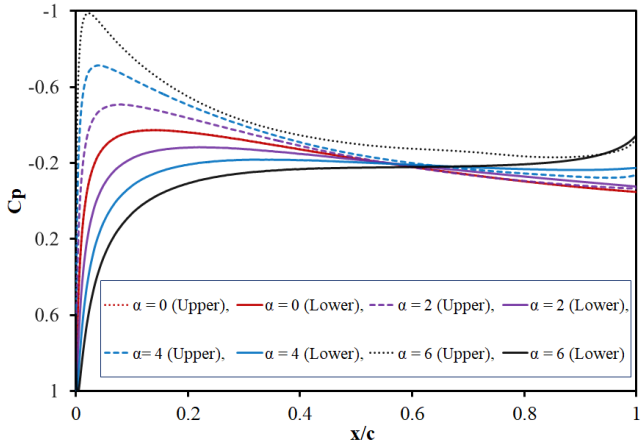

FIGURE 6. Distributions of pressure coefficient at various angle of attack.

the previous research work and hence the present method is validated.

B. COEFFICIENT OF PRESSURE DISTRIBUTION

Figure 6 displays the pressure coefficients classification over the upper and lower surfaces of the NACA0012 airfoil at a different angle of attack. From Fig. 6, this is noticed that as the angle of attack raised, suction manages increasing on the leading edge of the upper part of the airfoil and its peak curve position reaches to the leading edge. Moreover, the stagnation point of the airfoil at $C_p = 1$ with 0° angle of attack over the leading edge is deranged downstream from the airfoil on the lower surface, while at a 6° angle of attack, the stagnation point is located on the lower surface. Coefficients of pressure distribution is validated by Swanson and Langer [35] as shown in Fig. 7. Our results are in good agreement with the experimental data which shows that the presented algorithm is efficient for studying the transient flow over the airfoil.

C. FORMATION OF SEPARATION BUBBLE

Figure 8 displays the repelling and attracting LCSs over NACA0012 airfoil, the red lines denote the unstable

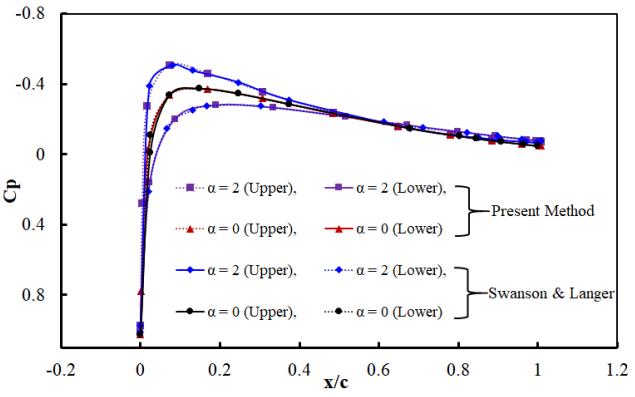

FIGURE 7. Pressure distribution literature comparison with the present method.

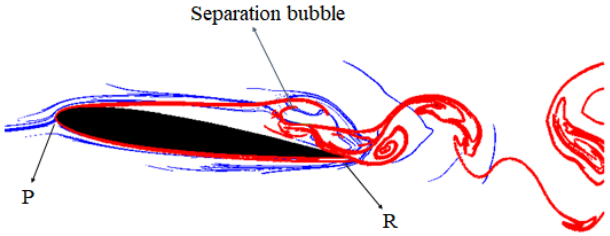

FIGURE 8. Contour plots of separation bubble structure.

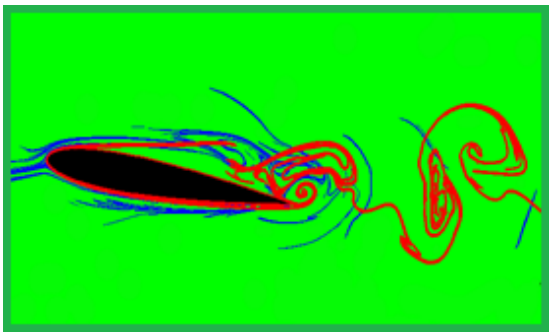

FIGURE 9. Contour plots of FTLE over airfoil displaying stable (blue) and unstable (red) manifolds.

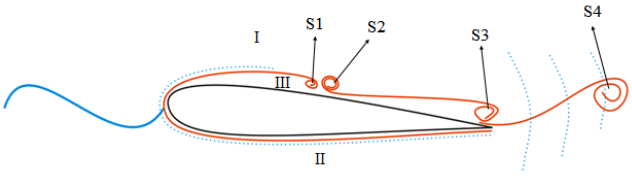

FIGURE 10. Schematic diagram of stable and unstable manifolds near the surface of airfoil (The red and blue lines denote the unstable and stable manifolds respectively).

manifolds, and the blue lines the stable manifolds. Transport barriers of repelling LCSs divided the upward flow into two parts. The flow adjacent to the airfoil is transferred into the separation bubble to form a vortex shedding. Thereafter, a number of flow particles from upstream with

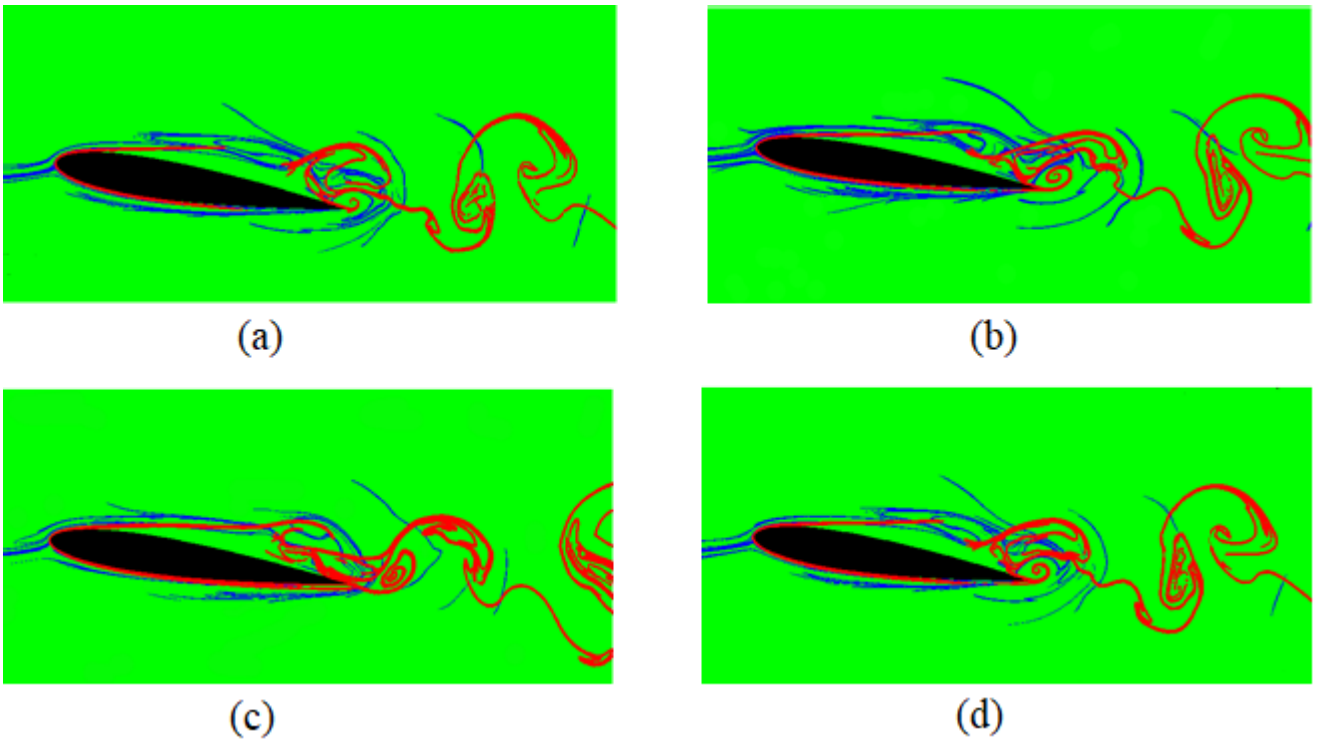

FIGURE 11. Contour plots of stable and unstable manifolds near the surface of airfoil (a) t = 0T, (b) t = 0.35T, (c) t = 0.70T and (d) t = T in a period.

immense kinetic energy would be transferred into the separation bubble. From Fig. 8, vorticity is carried into the separation bubble in addition to the fluid transport. P is considered as the separation point and R is the reattachment point of the flow.

D. STABLE AND UNSTABLE MANIFOLD OF AIRFOIL

The detailed discussion of area or lobes of definite particle mixing is explained by the stable and unstable manifolds. Therefore, a thorough understanding of the flow topology, it is required to combine the two to know how they merge. Stable and unstable manifolds combinations will uncover the true vortex boundaries, regions where entrainment is viable with a time-dependent profile of the separation bubble. The limited time evolution of the manifolds is shown in Fig. 9. For this case, we have computed the cognizant structure of the unstable manifolds with a contour map of the FTLE, and further enclosed a clipped contour map of the stable manifolds. Overall a thorough map of the manifolds is expressed in vortex shedding. Mostly, manifolds encounter and occasionally overlap. It validates that the flow boundaries are the mixture of stable/unstable manifolds. The more readable and complex behavior occurs inside the separation bubble. It is displayed in schematic Fig. 10. The stable manifold P divides the fluid near the leading edge of the airfoil into two regions I and II. The fluid in the region I flow over the airfoil to the downstream, and the fluid in region II flows beneath the airfoil. Region III is the energy exchange region between the separation bubble and the main flow I.

In Fig. 10, the impact of manifold S_3 can be seen. This manifold segregates the creation of region from the whole flow except the inlet during vortex formation. The novel vortices would show their stability from S_3 and separate it. With time changes, manifolds S_1, S_2 and S_3 adopt more defined as S_4 is eroding. Hence, manifold S_3 has lessened its defining shape, on the other hand, S_1 and S_2 manifolds have attained original shapes. Here, the formation of manifolds in action is generated. S_1, S_2, S_3 and S_4 are forming manifolds periodically that separate pairs of vortices from each other. This evolution of manifolds is continuously working and no longer contain their initial features.

Figure 11 shows the changes of stable/unstable manifolds and the position of the particles around the surface of the airfoil in a period. The farthest upstream unstable manifold which attaches to the airfoil is the separation point in the flow. This manifold is well defined and observed to be largely time invariant. The manifolds coincide with forming vortices and have a well-defined structure, form an attachment between the vortices. Finally, we have found that the reattachment profile periodically develops and propagates downstream to be shed with a vortex as a new reattachment profile forms upstream.

Following the physical meaning, LCSs and KAM tori can be considered as the boundary or barriers of the flow area. The method which is briefly described to identify tori is based on

the calculation of FTLE in forward and backward time. This method is defined to identify KAM tori like LCSs is apparent: these structures are described as trenches of FTLE fields that cohere in forward/backward time calculations.

VI. CONCLUSION

In the present analysis, we show the significance of KAM tori and the associated robust transport barriers. From the dynamical presepective, Lagrangian behavior of fluid is studied extensively. We also performed the flow topology for low Reynolds number, unsteady flow in the wake of an airfoil. The transport process in terms of Lagrangian dynamics has been analyzed based on KAM theory, stable and unstable manifold structures, and LCSs. We have used a numerical technique applicable for the detection of invariant manifolds of hyperbolic trajectories. The applied technique is based on the calculation of FTLE. We give additional insight into vortex shedding phenomena based on Lagrangian coherent structures (LCSs). There is not much research on the comprehensive mass transport phenomena near the wake of the airfoil. The present work focuses on the complete mass transport and mixing phenomena which would show more intuitively and concretely from the Lagrangian point of view. The importance of the process on the stable and unstable manifolds near the airfoil are analyzed in depth. The results show that stable and unstable manifolds could be mixed with each other as time evolves, and the KAM tori are generated to induce the transport process between the main flow and separation bubble. We have also examined that the mixing of unstable and stable manifolds can be used to detect vortex boundary. These manifolds can be used to trace vortex shedding, development, and evolution. As a result, it is concluded that Lagrangian analysis based on LCSs would give a deep insight into the dynamics of a vortex, which plays a significant role in understanding the unsteady aerodynamics of fluid flow. A comprehensive explanation of the mass transport process can contribute a new perspective for the investigation of the transient fluid flow.

REFERENCES

[1] G. Haller and G. Yuan, "Lagrangian coherent structures and mixing in two-dimensional turbulence," *Phys. D, Nonlinear Phenomena*, vol. 147, nos. 3–4, pp. 352–370, Dec. 2000.

[2] C. Garth, F. Gerhardt, X. Tricoche, and H. Hans, "Efficient computation and visualization of coherent structures in fluid flow applications," *IEEE Trans. Vis. Comput. Graphics*, vol. 13, no. 6, pp. 1464–1471, Nov. 2007.

[3] F. J. Beron-Vera, M. J. Olascoaga, M. G. Brown, H. Koçak, and I. I. Rypina, "Invariant-tori-like Lagrangian coherent structures in geophysical flows," *Chaos, Interdiscipl. J. Nonlinear Sci.*, vol. 20, no. 1, Mar. 2010, Art. no. 017514.

[4] M. Michini, M. A. Hsieh, E. Forgoston, and I. B. Schwartz, "Robotic tracking of coherent structures in flows," *IEEE Trans. Robot.*, vol. 30, no. 3, pp. 593–603, Jun. 2014.

[5] G. Haller, "A variational theory of hyperbolic Lagrangian coherent structures," *Phys. D, Nonlinear Phenomena*, vol. 240, no. 7, pp. 574–598, Mar. 2011.

[6] S. Kovalyov, "Phase space structure and anomalous diffusion in a rotational fluid experiment," *Chaos, Interdiscipl. J. Nonlinear Sci.*, vol. 10, no. 1, pp. 153–165, Mar. 2000.

[7] R. de la Llave, "A tutorial on KAM theory, in proceedings of symposia in pure mathematics," *J. Amer. Math. Soc.*, vol. 69, pp. 175–296, Jan. 2001.

[8] V. I. Arnold and B. A. Khesin, *Topological Methods in Hydrodynamics*. New York, NY, USA: Springer, 1998.

[9] L. J. Pratt, I. I. Rypina, T. M. Özgökmen, P. Wang, H. Childs, and Y. Bebieva, "Chaotic advection in a steady, three-dimensional, ekman-driven eddy," *J. Fluid Mech.*, vol. 738, pp. 143–183, Jan. 2014.

[10] S. Wiggins, *Normally Hyperbolic Invariant Manifolds in Dynamical Systems*. New York, NY, USA: Springer, 1994.

[11] V. Rom-Kedar, A. Leonard, and S. Wiggins, "An analytical study of transport, mixing and chaos in an unsteady vortical flow," *J. Fluid Mech.*, vol. 214, pp. 347–394, May 1990.

[12] G. Haller, "Lagrangian coherent structures from approximate velocity data," *Phys. Fluids*, vol. 14, no. 6, pp. 1851–1861, Jun. 2002.

[13] G. Haller, "Finding finite-time invariant manifolds in two-dimensional velocity fields," *Chaos, Interdiscipl. J. Nonlinear Sci.*, vol. 10, no. 1, pp. 99–108, Mar. 2000.

[14] G. Haller, "An objective definition of a vortex," *J. Fluid Mech.*, vol. 525, pp. 1–26, Feb. 2005.

[15] M. Mathur, G. Haller, T. Peacock, J. E. Ruppert-Felsot, and H. L. Swinney, "Uncovering the Lagrangian skeleton of turbulence," *Phys. Rev. Lett.*, vol. 98, no. 14, Apr. 2007, Art. no. 144502.

[16] S. C. Shadden, O. John, J. E. Marsden, and E. Jerrold, "Lagrangian analysis of fluid transport in empirical vortex ring flows," *Phys. Fluids*, vol. 18, no. 4, pp. 105–111, 2006.

[17] F. Lekien, C. Coulliette, A. J. Mariano, E. H. Ryan, L. K. Shay, G. Haller, and J. Marsden, "Pollution release tied to invariant manifolds: A case study for the coast of florida," *Phys. D, Nonlinear Phenomena*, vol. 210, nos. 1–2, pp. 1–20, Oct. 2005.

[18] I. I. Rypina, M. G. Brown, F. J. Beron-Vera, H. Koçak, M. J. Olascoaga, and I. A. Udovydchenkov, "Robust transport barriers resulting from strong Kolmogorov-Arnold-Moser stability," *Phys. Rev. Lett.*, vol. 98, no. 10, Mar. 2007, Art. no. 104102.

[19] M. J. Olascoaga, I. I. Rypina, M. G. Brown, F. J. Beron-Vera, H. Koçak, L. E. Brand, G. R. Halliwell, and L. K. Shay, "Persistent transport barrier on the West Florida Shelf," *Geophys. Res. Lett.*, vol. 33, no. 22, 2006, Art. no. L22603.

[20] S. Wiggins, "The dynamical systems approach to Lagrangian transport in oceanic flows," *Annu. Rev. Fluid Mech.*, vol. 37, no. 1, pp. 295–328, Jan. 2005.

[21] C. Coulliette and S. Wiggins, "Intergyre transport in a wind-driven, quasi geostrophic double gyre: An application of lobe dynamics," *Nonlinear Processes Geophys.*, vol. 8, no. 1, pp. 69–94, 2001.

[22] P. D. Miller, C. K. R. T. Jones, A. M. Rogerson, and L. J. Pratt, "Quantifying transport in numerically generated velocity fields," *Phys. D, Nonlinear Phenomena*, vol. 110, nos. 1–2, pp. 105–122, Dec. 1997.

[23] P. D. Miller, L. J. Pratt, K. R. Helfrich, and C. K. R. T. Jones, "Chaotic transport of mass and potential vorticity for an island recirculation," *J. Phys. Oceanogr.*, vol. 32, no. 1, pp. 80–102, Jan. 2002.

[24] I. I. Rypina, "Lagrangian coherent structures and transport in two-dimensional incompressible flows with oceanographic and atmospheric applications," Ph.D. dissertation, Univ. Miami, Coral Gables, FL, USA, 2007.

[25] A. Prykarpatski, O. Hentosh, and Y. Prykarpatsky, "Geometric structure of the classical Lagrange-d'Alambert principle and its application to integrable nonlinear dynamical systems," *Mathematics*, vol. 5, no. 4, p. 75, Dec. 2017.

[26] L. L. Van Dommelen and S. J. Cowley, "On the Lagrangian description of unsteady boundary-layer separation. Part 1. General theory," *J. Fluid Mech.*, vol. 210, pp. 593–626, Jan. 1990.

[27] J. Duan and S. Wiggins, "Lagrangian transport and chaos in the near wake of the flow around an obstacle: A numerical implementation of lobe dynamics," *Nonlinear Processes Geophys.*, vol. 4, no. 3, pp. 125–136, Sep. 1997.

[28] Z. J. Zhang, "Identification of Lagrangian coherent structures around swimming jellyfish from experimental time-series data," Ph.D. dissertation, California Inst. Technol., Pasadena, CA, USA, 2008.

[29] M. Farazmand, "A variational approach to coherent structures in unsteady dynamical systems," Ph.D. dissertation, ETH Zürich, Zürich, Switzerland, 2014.

[30] D. Lipinski, B. Cardwell, and K. Mohseni, "A lagrangian analysis of a two-dimensional airfoil with vortex shedding," *J. Phys. A, Math. Theor.*, vol. 41, no. 34, Aug. 2008, Art. no. 344011.

[31] I. I. Rypina, M. G. Brown, F. J. Beron-Vera, H. Kocak, M. J. Olascoaga, and I. A. Udovydchenkov, "On the Lagrangian dynamics of atmospheric zonal jets and the permeability of the stratospheric polar vortex," *J. Atmos. Sci.*, vol. 64, no. 3595, pp. 3593–3610, 2007.
[32] S. C. Shadden, F. Lekien, and J. E. Marsden, "Definition and properties of Lagrangian coherent structures from finite-time Lyapunov exponents in two-dimensional aperiodic flows," *Phys. D, Nonlinear Phenomena*, vol. 212, nos. 3–4, pp. 271–304, Dec. 2005.
[33] P. Nithiarasu, "An efficient artificial compressibility (AC) scheme based on the characteristic based split (CBS) method for incompressible flows," *Int. J. Numer. Methods Eng.*, vol. 56, no. 13, pp. 1815–1845, Apr. 2003.
[34] C. L. Ladson, "Effects of independent variation of Mach and Reynolds numbers on low speed aerodynamic characteristics of NACA 0012 airfoil section," NASA Langley Res. Centre, Hampton, VA, USA, Tech. Rep. NASA TM-4074, 1988.
[35] R. C. Swanson and S. Langer, "Comparison of NACA 0012 Laminar flow solutions: Structured and unstructured grid methods," NASA Langley Res. Centre, Hampton, VA, USA, Tech. Rep. NASA/TM-2016-219003, 2016.

RIAZ AHMAD received the B.Sc. degree from Bahauddin Zakariya University, Pakistan, in 2002, the master's degree in mathematics from Quaid-i-Azam University, Islamabad, Pakistan, in 2005, the M.S. degree in applied mathematics from the University of Engineering and Technology, Lahore, Pakistan, in 2014, and the Ph.D. degree in applied mathematics from Xi'an Jiaotong University, Xian, China. His research interests include Lagrangian description for unsteady flow, the Lagrangian coherent structure in the fluid flow, study fluid dynamics on manifolds, vortex dynamics analysis in Lagrangian frame, and KAM theory.

ASMA FAROOQI received the B.Sc. degree from Punjab University, Pakistan, in 2002, the master's degree in mathematics from Quaid-i-Azam University, Islamabad, Pakistan, in 2005, and the M.S. degree in applied mathematics from the University of Engineering and Technology Lahore, Lahore, Pakistan, in 2014. She is currently pursuing the Ph.D. degree in turbo-machinery aerodynamics from Xi'an Jiaotong University, Xi'an, China. Her research interests include numerical analysis, bio-mathematics, and control theory and optimization.

JIAZHONG ZHANG received the B.Sc. degree from Xi'an Jiaotong University, China, in 1990, the master's degree in mathematics from Xi'an Jiaotong University, China, in 1993, and the Ph.D. degree in architectural engineering and mechanics from Xi'an Jiaotong University, Xi'an, China, in 1997. He is currently a Professor with Xi'an Jiaotong University. His research interests include nonlinear aeroelastic stability and flow control by the morphing structure, and turbo-machinery or fluid machinery with low Reynolds number by smart structures.

ILYAS KHAN received the Ph.D. degree in applied mathematics from the Universiti Teknologi Malaysia, one of the world leading Universities. He has more than 15 years of academic experience in different reputed institutions of the world. He is currently an Associate Professor with the Department of Mathematics, Majmaah University, Saudi Arabia. He is also associated with Ton Duc Thang University, Vietnam, as a Researcher. He has published more than 500 research articles in different well-reputed international journals. His areas of interests include fluid dynamics, MHD flows, nanofluids, fractional derivatives, integral transforms, exact solutions, and mathematical modeling. He is the potential reviewer of many research journals of the world.

EL-SAYED M. SHERIF is currently a Full Professor with the Center of Excellence for Research in Engineering Materials (CEREM), Advanced Manufacturing Institute (AMI), King Saud University, Riyadh, Saudi Arabia. He is also a member of the American Nano Society (ANS). He has authored several books and articles. His research interests include material engineering, nanomaterials, and nanofluids. He is an editor and reviewer of several journals.